Efficient Acquisition Algorithm for Long Pseudorandom Sequence

WAN-HSIN HSIEH
National Chiao Tung University, Taiwan

CHIEH-FU CHANG
National Applied Research Laboratory - National Space Organization
Taiwan

MING-SENG KAO
National Chiao Tung University
Taiwan

In this paper, a novel method termed the phase coherence acquisition (PCA) is proposed for pseudorandom (PN) sequence acquisition. By employing complex phasors, the PCA requires only complex additions in the order of N, the length of the sequence, whereas the conventional method using fast Fourier transform (FFT) requires complex multiplications and additions both in the order of $N \log_2 N$. To combat noise, the input and local sequences are partitioned and mapped into complex phasors in PCA. The phase differences between pairs of input and local phasors are used for acquisition; thus, complex multiplications are avoided. For more noise-robustness capability, the multilayer PCA is developed to extract the code phase step-by-step. The significant reduction of computational loads makes the PCA an attractive method, especially when the sequence length of N is extremely large, which becomes intractable for the FFT-based acquisition.

Manuscript received July 30, 2012; revised March 9 and July 27, 2013; released for publication September 21, 2013.

DOI. No. 10.1109/TAES.2014.120460.

Refereeing of this contribution was handled by W. Blanding.

Authors' current addresses: W.-H. Hsieh, Applied Research Department, St. Jude Medical, Inc., Taipei, Taiwan E-mail: (hsieh1979@gmail.com); C.-F. Chang, Electrical Engineering Division, National Applied Research Laboratory - National Space Organization, Hsinchu, Taiwan; M.-S. Kao, Communication Engineering Department, National Chiao Tung University, Hsinchu, Taiwan.

I. INTRODUCTION

Pseudorandom (PN) sequence matching is widely used in various applications. For example, in spread-spectrum communications and global navigation satellite system (GNSS) receivers, the matching is implemented to search for the correct code phase so as to identify the transmitter. The serial search acquisition for matching the PN sequence by finding the correlation peak is simple and straightforward, but it is rather time-consuming with exhaustive searches required for each code phase [1, 2]. Because the correlation of the PN sequence in the acquisition can be calculated by using the convolution theorem and implemented with the fast Fourier transform (FFT) algorithm, parallel search acquisition based on the FFT algorithm is proposed to significantly reduce acquisition time, but this results in an increase in complexity [3–7]. Specifically, the convolution of two sequences can be derived from the pointwise product of the corresponding Fourier transforms (i.e., $x[n] \otimes y[n] \xrightarrow{F} X(\omega) \cdot Y(\omega)$, where $\otimes$ denotes the convolution and F represents the Fourier transform).

The previous works regarding the reduction of complexity or computation of PN sequence acquisition using the FFT algorithm mainly focused on reducing the number of input elements either in the FFT stage (by summing over a number of chips or superimposing folded segments of the local code), in the inverse FFT (IFFT) stage (by performing only on the portion of data with significant power), or in combination with the Doppler search [8–14]. The FFT/IFFT structure basically remains and serves as the intermediate component for facilitating the search for the code phase. Hence, the computation load for acquisition is dominated by the computation of FFT/IFFT that involves a number of complex multiplications [3–5].

In this paper, we propose an approach, termed phase coherence acquisition (PCA), which uses a distinct perspective from the conventional FFT/IFFT structure. That is, the PCA extracts the desired code phase information by using phasors in the complex domain. Owing to the simple phase manipulation of phasors and the elimination of inverse mapping into the time domain, the PCA requires much less computation than FFT-based acquisition to search for the correlation peak of PN sequences. It is noteworthy that PCA requires no multiplication as compared with FFT-based acquisition. This superiority becomes prominent when the applied sequence length N is very large such that the FFT-based approach is difficult to be implemented. This paper is organized as follows. First, we describe the motivation of our work. Next, we develop our approach in the noiseless case and provide the essential idea in our development. To achieve noise robustness, we then incorporate a novel segmentation scheme in our approach and propose the PCA method. The simulation results are provided to verify the analysis and demonstrate the performance of the

proposed method. Finally, the computation of PCA and FFT-based method are discussed.

II. MOTIVATION

The convolution theorem states that under general conditions, the Fourier transform of a convolution between two sequences is the pointwise product of the Fourier transforms of these two sequences. The theorem can be represented by

$$F\{x[n] \otimes y[n]\} = F\{x[n]\} \cdot F\{y[n]\}, \tag{1}$$

where F denotes Fourier transform. By applying the inverse Fourier transform F^{-1}, we have

$$x[n] \otimes y[n] = F^{-1}\{F\{x[n]\} \cdot F\{y[n]\}\}. \tag{2}$$

In many applications, the code phase search between two sequences is usually implemented by FFT and its inverse due to the efficient computation compared with the exhaustive direct serial search method. The computation of FFT of N points involves complex multiplications and additions of order $N \log_2 N$. Due to the diverse need for applications and the increasing complexity of modern algorithms, a more computationally efficient method is needed when the length of processed sequence becomes so large that implementation using the FFT method becomes difficult. Our idea for code phase acquisition that attains much less computation is developed in the following.

III. ACQUISITION BY PHASOR

Let $S_{IN} = \{x_0, x_1, \cdots, x_{N-1}\}$ and $S_{LO} = \{y_0, y_1, \cdots, y_{N-1}\}$ be the input and local PN sequences of length N, respectively, where $x_n, y_n \in \{1, -1\}$. In noiseless condition, the cross correlation between $\{x_n\}$ and $\{y_n\}$ is denoted by

$$C(m) = \sum_{k=0}^{N-1} x_{k+m} y_k, \tag{3}$$

where $m = 0, 1, \cdots N-1$.

Let the code phase shift between S_{IN} and S_{LO} be q, where $q \in \{0, 1, \cdots, N-1\}$. We first map the input and local sequences into phasors as given by

$$X = \sum_{n=0}^{N-1} x_n \gamma^{-n} \tag{4}$$

$$Y = \sum_{n=0}^{N-1} y_n \gamma^{-n}, \tag{5}$$

where $\gamma = e^{j\frac{2\pi}{N}}$ and $j = \sqrt{-1}$.

We then calculate

$$\begin{aligned}\Pi &= X^* \cdot Y \\ &= \left(\sum_{n=0}^{N-1} x_n \gamma^{n}\right) \cdot \left(\sum_{k=0}^{N-1} y_k \gamma^{-k}\right) \\ &= \left(\sum_{m=0}^{N-1} x_{k+m} \gamma^{k+m}\right) \cdot \left(\sum_{k=0}^{N-1} y_k \gamma^{-k}\right) \\ &= \sum_{m=0}^{N-1} \sum_{k=0}^{N-1} x_{k+m} y_k \gamma^{m} \\ &= \sum_{m=0}^{N-1} \gamma^m C(m), \end{aligned} \tag{6}$$

where the superscript $*$ denotes the complex conjugation and $C(m)$ represents the cross correlation between $\{x_n\}$ and $\{y_n\}$. To present our concept in a direct and effective manner, the maximal-length sequence (MLS) is illustrated for the sequence acquisition. The cross correlation between $\{x_n\}$ and $\{y_n\}$ is given by

$$C(m) = \begin{cases} N, & \text{if } m = q, \\ -1, & \text{if } m \neq q. \end{cases} \tag{7}$$

Hence, (6) becomes

$$\begin{aligned}\Pi &= \sum_{m=0}^{N-1} \gamma^m C(m) \\ &= C(q)\gamma^q + \sum_{m=0, m\neq q}^{N-1} \gamma^m C(m) \\ &= (N+1)\gamma^q - \sum_{m=0}^{N-1} \gamma^m \\ &= (N+1)\gamma^q \\ &= (N+1)e^{j\frac{2\pi}{N}q}, \end{aligned} \tag{8}$$

where the equality $\sum_{m=0}^{N-1} \gamma^m = 0$ is applied in the above derivation.

Let the phase of Π be Ψ as denoted by

$$\Psi = \frac{2\pi}{N} q. \tag{9}$$

The acquisition of the sequence can then be achieved by

$$q = \frac{N}{2\pi} \Psi. \tag{10}$$

Because the input sequence consists of $+1$ and -1, the complex phasor of (4) is obtained by simply N additions (subtractions). Note that the computations of the phasor regarding the local sequence can be omitted by calculating (5) in advance.

In the above derivation, when the phasor of the input sequence is obtained by (4), very few computations are needed to determine the shift q, that is, much fewer than those required for the FFT-based approach. However, the phase accuracy of the complex phasor is sensitive to noise. The phase resolution is $2\pi/N$ according to (9). As shown in Fig. 1, when N is large, the distance between adjacent phases is rather small, which easily leads to erroneous phase estimation under the noisy environment. Hence, it becomes necessary to design an algorithm that permits the

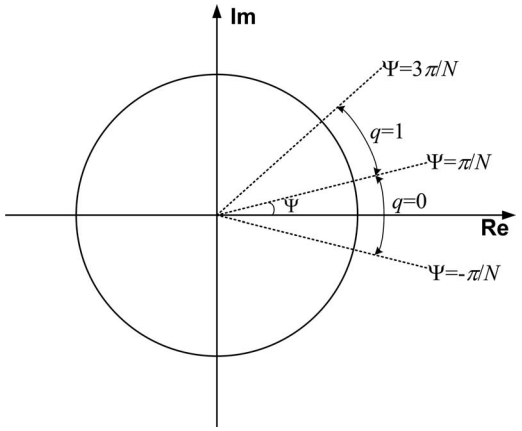

Fig. 1. Schematic plot of phase resolution for phasors on complex domain.

distance between adjacent phases to be increased to resist the effect of noise.

IV. PCA

A. Segmentation

Suppose the input sequence S_{IN} has the length of $N = K \cdot M$. In the PCA, S_{IN} is first partitioned into K-disjointed segments of length M as denoted by

$$\begin{aligned}
&\mathbf{A_0} = \{x_0, x_K, x_{2K}, \cdots x_{(M-1)K}\}\\
&\mathbf{A_1} = \{x_1, x_{K+1}, x_{2K+1}, \cdots x_{(M-1)K+1}\}\\
&\vdots\\
&\mathbf{A_{K-1}} = \{x_{K-1}, x_{2K-1}, x_{3K-1}, \cdots x_{MK-1}\}\\
&\quad = \{x_{K-1}, x_{2K-1}, x_{3K-1}, \cdots x_{N-1}\}.
\end{aligned} \tag{11}$$

Similarly, the local sequence S_{LO} is also partitioned into K-disjointed segments as below:

$$\begin{aligned}
&\mathbf{B_0} = \{y_0, y_K, y_{2K}, \cdots y_{(M-1)K}\}\\
&\mathbf{B_1} = \{y_1, y_{K+1}, y_{2K+1}, \cdots y_{(M-1)K+1}\}\\
&\vdots\\
&\mathbf{B_{K-1}} = \{y_{K-1}, y_{2K-1}, y_{3K-1}, \cdots y_{MK-1}\}\\
&\quad = \{y_{K-1}, y_{2K-1}, y_{3K-1}, \cdots y_{N-1}\}.
\end{aligned} \tag{12}$$

Suppose the code phase shift between the input and the local sequences is $q = cK + d$, where $0 \le c < M$ and $0 \le d < K$. We then have $y_i = x_{i+q} = x_{i+cK+d}$, and the following relationships

$$\begin{aligned}
&\mathbf{B_0} = \{y_0, y_K, y_{2K}, \cdots y_{(M-1)K}\}\\
&\quad = \{x_{cK+d}, x_{(c+1)K+d}, \cdots, x_{(M-1)K+d}, x_d, \cdots, x_{(c-1)K+d}\}\\
&\quad = \mathbf{A_d}(c)\\
&\mathbf{B_1} = \mathbf{A_{d+1}}(c)\\
&\vdots\\
&\mathbf{B_{K-d-1}} = \mathbf{A_{K-1}}(c),
\end{aligned} \tag{13}$$

where $\mathbf{A_d}(c)$ denotes the circular shift of $\mathbf{A_d}$ with c chips to left.

The remaining $\mathbf{B_{K-d}}, \mathbf{B_{K-d+1}}, \cdots, \mathbf{B_{K-1}}$ can be derived by using the same logics but with adjustments, as given by

$$\begin{aligned}
&\mathbf{B_{K-d}} = \{y_{K-d}, y_{2K-d}, y_{3K-d}, \cdots y_{MK-d}\}\\
&\quad = \{x_{(K-d)+cK+d}, x_{(2K-d)+cK+d}, \cdots, x_{MK+d+cK+d}\}\\
&\quad = \{x_{(c+1)K}, x_{(c+2)K}, \cdots, x_0, \cdots, x_{cK}\}\\
&\quad = \mathbf{A_0}(c+1)\\
&\mathbf{B_{K-d+1}} = \mathbf{A_1}(c+1)\\
&\vdots\\
&\mathbf{B_{K-1}} = \mathbf{A_{d-1}}(c+1).
\end{aligned} \tag{14}$$

From (13) and (14), the relationships between $\mathbf{A_i}$ and $\mathbf{B_i}$ can be generalized as follows:

$$\begin{aligned}
\mathbf{B_i} &= \mathbf{A_{d+i}}(c), \quad 0 \le i \le K-d-1\\
&= \mathbf{A_{(d+i) \bmod K}}(c+1), \quad K-d \le i \le K-1.
\end{aligned} \tag{15}$$

B. Acquisition by Phase

In each segment of (11) and (12), we map the sequences into the complex phasors by

$$X_i = \sum_{n=0}^{M-1} x_{nK+i}\alpha^{-n} \tag{16}$$

$$Y_i = \sum_{n=0}^{M-1} y_{nK+i}\alpha^{-n}, \tag{17}$$

where $\alpha = e^{j\frac{2\pi}{M}}$ and $i = 0, 1, 2, \cdots K-1$.

Let $\mathbf{A_i}(m)$ be the segment $\mathbf{A_i}$ with m circular shifts to left, denoted by

$$\mathbf{A_i}(m) = \{x_{mK+i}, x_{(m+1)K+i}, \cdots, x_i, \cdots, x_{(m-1)K+i}\}. \tag{18}$$

Accordingly, the complex phasor pertaining to $\mathbf{A_i}(m)$ is given by

$$\begin{aligned}
X_i(m) &= \sum_{n=0}^{M-1} x_{(m+n)K+i}\alpha^{-n}\\
&= \sum_{n=0}^{M-1} x_{(m+n)K+i}\alpha^{-(m+n)} \cdot \alpha^m\\
&= \alpha^m \sum_{u=0}^{M-1} x_{uK+i}\alpha^{-u}\\
&= \alpha^m X_i.
\end{aligned} \tag{19}$$

According to (19) and (15), the complex phasors Y_i are derived by

$$\begin{aligned}
Y_i &= \alpha^c \cdot X_{d+i}\\
&= e^{j\frac{2\pi}{M}c} \cdot X_{d+i}, \quad 0 \le i \le K-d-1
\end{aligned} \tag{20}$$

$$\begin{aligned}
Y_i &= \alpha^{c+1} \cdot X_{d+i}\\
&= e^{j\frac{2\pi}{M}(c+1)} \cdot X_{d+i}, \quad K-d \le i \le K-1.
\end{aligned} \tag{21}$$

Furthermore, the complex phasors X_i and Y_i can be expressed by

$$X_i = |X_i|e^{j\theta_i} \tag{22}$$

$$Y_i = |Y_i|e^{j\phi_i}, \tag{23}$$

where θ_i and ϕ_i denote the phases of X_i and Y_i, respectively.

From (20) to (23), we have the following phase relationship:

$$\begin{aligned}\phi_i &= \theta_{i+d} + \frac{2\pi}{M}\cdot c, \quad 0 \le i \le K-d-1 \\ &= \theta_{i+d} + \frac{2\pi}{M}\cdot (c+1), \quad K-d \le i \le K-1. \end{aligned} \tag{24}$$

Let G_m be the sum of the K complex phasors, defined as

$$G_m = \sum_{i=0}^{K-m-1} e^{j(\phi_i - \theta_{i+m})} + \sum_{i=K-m}^{K-1} e^{j(\phi_i - \theta_{i+m} - \frac{2\pi}{M})}, \tag{25}$$

where $m = 0, 1, 2, \cdots K-1$.

According to the relationship of (24), when $m = d$, we have

$$\begin{aligned} G_d &= \sum_{i=0}^{K-m-1} e^{j(\phi_i - \theta_{i+d})} + \sum_{i=K-m}^{K-1} e^{j(\phi_i - \theta_{i+d} - \frac{2\pi}{M})} \\ &= K\cdot e^{j\frac{2\pi}{M}c}. \end{aligned} \tag{26}$$

Apparently,

$$|G_d| = K. \tag{27}$$

Note that we have a peak magnitude given by (27) when the K complex phasors are coherently added for G_d. On the other hand, when $m \neq d$, G_m is the sum of the K phasors of noncoherent phases, and the resultant magnitude is expected to be much smaller than K. Hence, the value of d can be obtained by finding the peak magnitude among $\{|G_m|\}$. In addition, let Θ be the phase of G_d. From (26), we have

$$\Theta = \frac{2\pi}{M}\cdot c. \tag{28}$$

Thus, c is given by

$$c = M\cdot\frac{\Theta}{2\pi}. \tag{29}$$

Let the estimates of (c, d) be $(\hat{c}, \hat{d})$. Practically, when $\hat{d} = d$ and $\hat{c}$ is equal to c, the shift $q = \hat{c}K + \hat{d}$ is correctly determined.

In PCA, the input sequence is one-bit quantized, partitioned, and transformed into phasors as given by (16). The phase differences between phasors of the input and local sequences are then used for the acquisition, as given by (25). When the phase differences between phasors are coherently added, we can have a large peak ($|G_d|$) to determine the correct segment for code phase acquisition. These processes simply require complex additions and eliminate the need for complex multiplications that are the major advantages of the PCA. The segmentation process confers noise robustness in the PCA method by the high correct probability of 1) $\hat{d} = d$, because of the coherent addition of K components, and 2) $\hat{c} = c$, because the noise effect is mitigated in determining phase of G_d with an enlarged distance between adjacent phases, i.e., from $2\pi/N$ to $2\pi/M$ by comparing (9) and (28). Hence, the ultimate accuracy of code phase acquisition is improved with the correct probability of $\hat{d}$ and $\hat{c}$ after the segmentation process. However, the estimated $(\hat{c}, \hat{d})$ could be erroneous when the signl-to-noise ratio (SNR) is very low, especially $\hat{c}$. In such situations, the multilayer scheme can be applied to enhance the noise resistance in the PCA method.

C. Multilayer PCA

In the multilayer PCA, the first-layer process is identical to the method described above. First, the input and local sequences of length N are partitioned into K_1 segments of length M_1, where $N = K_1M_1$. Assume the shift is denoted as $q = c_1K_1 + d_1$. In the first layer, only d_1 is estimated by finding the peak of $|G_m^{(1)}|$ in (25), and c_1 is left undetermined owing to the sensitivity to the effect of noise. The superscripts (1) and (2) in G_m indicate the first layer and the second layer, respectively. After the first layer is completed, we assume $\hat{d}_1 = d_1$ and

$$\begin{aligned}\mathbf{B_i} &= \mathbf{A}_{\hat{\mathbf{d}}_1+\mathbf{i}}(c_1), \quad 0 \le i \le K_1 - \hat{d}_1 - 1 \\ &= \mathbf{A}_{\hat{\mathbf{d}}_1+\mathbf{i}}(c_1+1), \quad K_1 - \hat{d}_1 \le i \le K_1 - 1, \end{aligned} \tag{30}$$

where c_1 is still undetermined.

We rewrite (30) by

$$\mathbf{B_i} = \mathbf{A'}_{\hat{\mathbf{d}}_1+\mathbf{i}}(c_1), \quad 0 \le i \le K_1 - 1 \tag{31}$$

where

$$\mathbf{A'}_{\hat{\mathbf{d}}_1+\mathbf{i}}(c_1) = \begin{cases} \mathbf{A}_{\hat{\mathbf{d}}_1+\mathbf{i}}(c_1), & 0 \le i \le K_1 - \hat{d}_1 - 1 \\ \mathbf{A}_{\hat{\mathbf{d}}_1+\mathbf{i}}(c_1+1), & K_1 - \hat{d}_1 \le i \le K_1 - 1. \end{cases}$$

From (31), all the pairs of $(\mathbf{A'}_{\hat{\mathbf{d}}_1+\mathbf{i}}, \mathbf{B}_i)$ have the same shift of c_1 chips in between, which is the key for the following derivation in the second layer.

The process of the second layer is introduced next. For simplicity, we take the pair $(\mathbf{A'}_{\hat{\mathbf{d}}_1}, \mathbf{B_0})$ as an example, where each $\mathbf{A'}_{\hat{\mathbf{d}}_1}$ and $\mathbf{B_0}$ contains M_1 elements and their relative shift is c_1, i.e., $\mathbf{B_0} = \mathbf{A'}_{\hat{\mathbf{d}}_1}(c_1)$. Let $M_1 = K_2 \cdot M_2$ and assume $c_1 = c_2K_2 + d_2$, where $0 \le c_2 \le M_2$ and $0 \le d_2 \le K_2$. First, $\mathbf{A'}_{\hat{\mathbf{d}}_1}$ and $\mathbf{B_0}$ are partitioned into K_2-disjointed segments of length M_2 as before. Following the same calculation as (25), the sum of the K_2 complex phasors is obtained for $(\mathbf{A'}_{\hat{\mathbf{d}}_1}, \mathbf{B_0})$, given as

$$H_{r,0} = \sum_{s=0}^{K_2-r-1} e^{j(\phi'_s - \theta'_{s+r})} + \sum_{s=K_2-r}^{K_2-1} e^{j(\phi'_s - \theta'_{s+r} - \frac{2\pi}{M_2})}, \tag{32}$$

where $r = 0, 1, \cdots, K_2 - 1$ and (ϕ'_s, θ'_s) are the corresponding phases involved in the calculation.

When $r = d_2$, we have $H_{d_2,0} = K_2 \cdot e^{j\frac{2\pi}{M_2}c_2}$ under the noiseless condition, which has the maximum magnitude among $\{H_{r,0}\}$.

When the similar calculation is applied to the other pairs $(\mathbf{A'}_{\hat{\mathbf{d}}_1+i}, \mathbf{B}_i)$, $i = 1, 2, \cdots, K_1 - 1$, their associated $H_{r,i}$ can then be obtained. Afterwards, all of the $H_{r,i}$ are

used to calculate

$$G_r^{(2)} = \sum_{i=0}^{K_1-1} H_{r,i}, \tag{33}$$

where $r = 0, 1, \cdots, K_2 - 1$.

Because all the pairs $(\mathbf{A}'_{\hat{\mathbf{d}}_1+i}, \mathbf{B}_i)$ have the same shift of c_1 chips in between, where $c_1 = c_2K_2 + d_2$, $G_{d_2}^{(2)}$ will have a peak magnitude among $\{G_r^{(2)}\}$. Specifically, in a noiseless condition, we have

$$\begin{aligned} G_{d_2}^{(2)} &= \sum_{i=0}^{K_1-1} H_{d_2,i} \\ &= \sum_{i=0}^{K_1-1} K_2 \cdot e^{j\frac{2\pi}{M_2}c_2} \\ &= K_1K_2 \cdot e^{j\frac{2\pi}{M_2}c_2}, \end{aligned} \tag{34}$$

where the peak magnitude is K_1K_2.

Similar to the first layer, by finding the peak magnitude among $\{|G_r^{(2)}|\}$, we can estimate d_2, which is denoted by $\hat{d}_2$. Let Φ be the phase of $G_{\hat{d}_2}^{(2)}$ as given by

$$\Phi = \frac{2\pi}{M_2} \cdot c_2. \tag{35}$$

Similar to (29), the estimate of c_2, denoted by $\hat{c}_2$, is obtained by

$$\hat{c}_2 = M_2 \cdot \frac{\Phi}{2\pi}. \tag{36}$$

According to (35), the separation between adjacent phases is further enlarged from $2\pi/M_1$ to $2\pi/M_2$, which significantly increases the resistance to noise. Note that c_2 can also be left undetermined after the second layer and determined by the third layer, if necessary. Nevertheless, from our simulation results, two layers appear to be sufficient for most applications. Finally, the estimate of q, denoted as $\hat{q}$, is calculated as

$$\begin{aligned} \hat{q} &= \hat{c}_1K_1 + \hat{d}_1 \\ &= (\hat{c}_2K_2 + \hat{d}_2)K_1 + \hat{d}_1. \end{aligned} \tag{37}$$

D. Error Detection Capability

When the segment of the first layer is correctly estimated, i.e., $\hat{d}_1 = d_1$, we obtain a much larger peak in the second layer for $\hat{d}_2 = d_2$. Taking the noiseless case, for example, we have the peak of K_1 in $|G_{d_1}^{(1)}|$, according to (26). In contrast, a much larger peak of K_1K_2 is obtained from $|G_{d_2}^{(2)}|$ in (34). As a result, the existence of a significant peak in $|G_r^{(2)}|$ of the second layer can be used to verify the correctness of $\hat{d}_1$, which shows the inherent error detection capability of PCA. Accordingly, correct $\hat{d}_1$ can be obtained with some recursive algorithms using such an error detection property, and the performance of the multilayer PCA can be further improved. This special feature has been verified in our simulations.

V. PERFORMANCE OF PCA

Let the input PN sequence be $\{x_n\}$. Assume the sequence is distorted by zero-mean Gaussian noise ζ_n with variance σ_ζ^2 and is one-bit quantized, as denoted by

$$w_n = \text{sign}(x_n + \zeta_n), \tag{38}$$

where $n = 0, 1, \cdots, N-1$, $\text{sign}(z) = 1$, if $z \geq 0$, and $\text{sign}(z) = -1$, if $z < 0$.

In the first layer, the input and local sequences, $\{w_n\}$ and $\{y_n\}$, are partitioned into K_1 segments of length M_1, as denoted by

$$\mathbf{A_i} = \{w_i, w_{K_1+i}, w_{2K_1+i}, \cdots w_{(M-1)K_1+i}\} \tag{39}$$

$$\mathbf{B_i} = \{y_i, y_{K_1+i}, y_{2K_1+i}, \cdots y_{(M-1)K_1+i}\}, \tag{40}$$

where $i = 0, 1, \cdots, K_1 - 1$.

Similar to (16) and (17), the complex phasors are defined by

$$\begin{aligned} W_i &= \sum_{n=0}^{M_1-1} w_{nK_1+i}\alpha^{-i} \\ &= |W_i|e^{j\theta_i} \end{aligned} \tag{41}$$

$$\begin{aligned} Y_i &= \sum_{n=0}^{M_1-1} y_{nK_1+i}\alpha^{-n} \\ &= |Y_i|e^{j\phi_i}. \end{aligned} \tag{42}$$

Moreover, according to (25), the sum of complex phasors is given by

$$\begin{aligned} G_m^{(1)} &= \sum_{i=0}^{K_1-m-1} e^{j(\phi_i-\theta_{i+m})} + \sum_{i=K_1-m}^{K_1-1} e^{j(\phi_i-\theta_{i+m}-\frac{2\pi}{M_1})} \\ &= \sum_{i=0}^{K_1-1} e^{j\psi_{i,m}}, \end{aligned} \tag{43}$$

where $\psi_{i,m}$ denotes the phase difference between the complex phasors W_{i+m} and Y_i, $-\pi \leq \psi_{i,m} \leq \pi$, and $m = 0, 1, \cdots, K_1$.

Let the shift between $\{w_n\}$ and $\{y_n\}$ be $q = c_1K_1 + d_1$. As derived in the Appendix, the magnitude of $|G_m^{(1)}|$ with $m \neq d_1$, i.e., the sidelobe, is a random variable with the Rayleigh distribution given by

$$f(r_s) = \frac{r_s}{K_1/2}e^{-r_s^2/K_1}, \tag{44}$$

where $f(r_s)$ is the probability density function of $|G_m^{(1)}|$ and $r_s \geq 0$.

In addition, $|G_m^{(1)}|$ with $m = d_1$, i.e., $|G_{d_1}^{(1)}|$, has the Rice distribution given by

$$f(r_p) = \frac{r_p}{\sigma_{p1}^2}e^{-(r_p^2+\mu_{\text{Re1}}^2)/2\sigma_{p1}^2} \cdot I_0\left(\frac{r_p\mu_{\text{Re1}}}{\sigma_{p1}^2}\right), \tag{45}$$

where $r_p \geq 0$.

For a given r_p, the probability of $r_p > r_s$ is denoted by

$$\Pr(r_p > r_s) = \int_0^{r_p} f(r_s)dr_s = 1 - \exp\left(-\frac{r_p^2}{K_1}\right). \quad (46)$$

Because there are $K_1 - 1$ sidelobes in the $G_m^{(1)}$, the correct d_1 is obtained when $|G_{d_1}^{(1)}|$is greater than all the other $K_1 - 1$ sidelobes. Hence, for a given r_p, the correct probability of detecting d_1 is given by

$$\mathrm{P_d}(r_p) = \left(1 - \exp\left(-\frac{r_p^2}{K_1}\right)\right)^{K_1-1}. \quad (47)$$

When the distribution of r_p is considered, the correct probability of d_1, i.e. $\hat{d}_1 = d_1$, is denoted by

$$\mathrm{P_{D1}} = \int_0^{\infty} \mathrm{P_d}(r_p) f(r_p) dr_p. \quad (48)$$

Furthermore, the probability of correct c_1 shall be considered for the correct acquisition in the one-layer PCA. According to (29), c_1 is obtained from the phase of $G_{d_1}^{(1)}$; thus, the probability of detecting c_1 can be derived in light of the phase distribution of $G_{d_1}^{(1)}$. Specifically, let the phase of $G_{d_1}^{(1)}$ be φ. For simplicity, assume $c_1 = 0$. According to the schematic concept shown in Fig. 1, c_1 is correct if $|\varphi| \le \frac{\pi}{M_1}$. Using the joint magnitude and phase distribution of $G_{d_1}^{(1)}$ derived in the Appendix, we have

$$f(r_p, \varphi) = \frac{r_p}{2\pi\sigma_{p1}^2} \exp\left(-\frac{r_p^2 + \mu_{\mathrm{Re1}}^2 - 2r_p\mu_{\mathrm{Re1}}\cos\varphi}{2\sigma_{p1}^2}\right), \quad (49)$$

where $-\pi \le \varphi < \pi$.

The joint probability of correct d_1 and c_1 is then denoted by

$$\mathrm{P_{C1}} = \Pr\left(\hat{d}_1 = d_1, |\varphi| \le \frac{\pi}{M_1}\right) = 2 \cdot \int_0^{\frac{\pi}{M_1}} \int_0^{\infty} \mathrm{P_d}(r_p) f(r_p, \varphi) dr_p d\varphi. \quad (50)$$

We use the MLS of length $N = 2^{20} - 1$ to verify the analysis. Let $K_1 = 2^{10} + 1$ and $M_1 = 2^{10} - 1$. The mentioned correct probabilities are simulated by the Monte Carlo method with 10 000 trials. The correct probabilities of $\mathrm{P_{D1}}$ and $\mathrm{P_{C1}}$ are shown in Figs. 2 and 3, respectively. In both figures, the analytical and simulated results are consistent with each other, which justifies the validity of our analysis. The correct probability of d_1 approaches one when SNR > -15 dB and begins to degrade with decreasing SNR. Note that the probability of d_1 is critical to the performance of PCA. The acquisition process will fail if d_1, i.e., the correct segment, cannot be correctly detected. On the other hand, the correct probability of $\mathrm{P_{C1}}$ is worse than $\mathrm{P_{D1}}$, which approaches one when SNR > 10 dB but drops to below 0.1 if SNR < 0 dB.

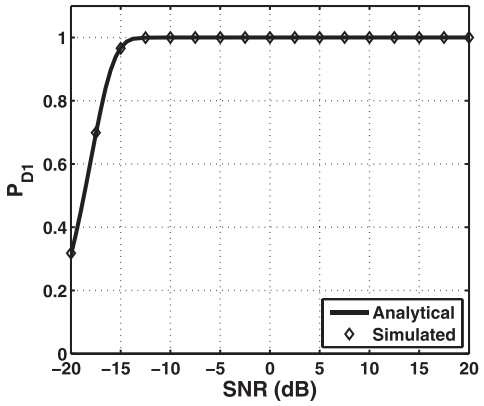

Fig. 2. Correct probability of d_1 in first layer of PCA.

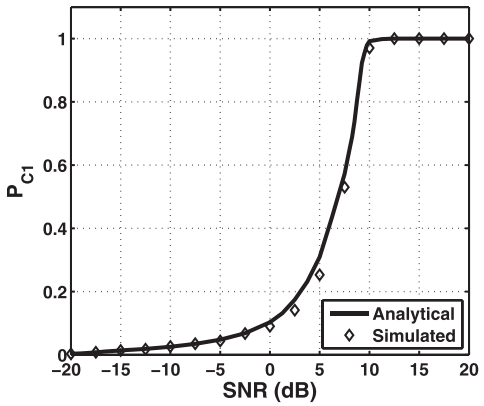

Fig. 3. Joint correct probability of d_1 and c_1 in first layer of PCA.

Besides the correct probability, the standard deviation (STD) of $\hat{c}_1$ is also derived to study the deviation of code phase shift. We consider the STD of $\hat{c}_1$ with the condition that $\hat{d}_1 = d_1$, which is denoted by

$$\sigma_\varphi = \left[\frac{1}{\mathrm{P_{D1}}} \int_{-\pi}^{\pi} \varphi^2 \cdot \int_0^{\infty} \mathrm{P_d}(r_p) f(r_p, \varphi) dr_p d\varphi\right]^{1/2}. \quad (51)$$

In Fig. 4, the STD decreases with SNR. Specifically, the STD of $\hat{c}_1$ is about four chips when SNR $= 0$ dB and decreases to within one chip for SNR ≥ 6 dB. According to the STD of $\hat{c}_1$, the one-layer PCA performs well only in the case of the high SNR. For applications with low SNR, the second layer is needed to improve performance in PCA.

Let $M_1 = K_2 M_2$ and $c_1 = c_2 K_2 + d_2$ in the second layer of PCA. According to (32) and (33), the sum of complex phasors is given by

$$G_n^{(2)} = \sum_{i=0}^{K_1-1} \left(\sum_{t=0}^{K_2-n-1} e^{j(\phi_{i,t} - \theta_{i,t+n})} + \sum_{t=K_2-n}^{K_2-1} e^{j(\phi_{i,t} - \theta_{i,t+n} - \frac{2\pi}{M_2})}\right) = \sum_{i=0}^{K_1-1} \sum_{t=0}^{K_2-1} e^{j\psi_{i,t+n}}, \quad (52)$$

where $n = 0, 1, \cdots, K_2$.

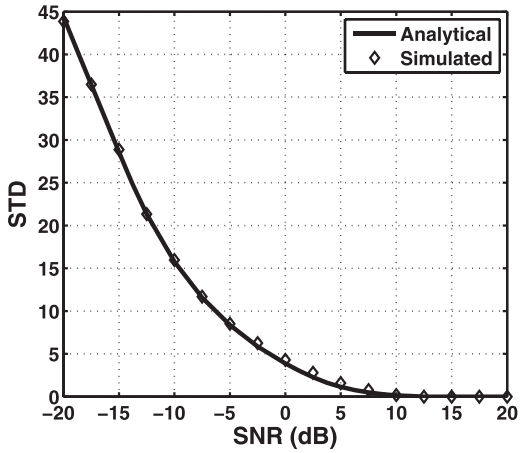

Fig. 4. STD of $\hat{c}_1$ in first layer of PCA, when $\hat{d}_1 = d_1$.

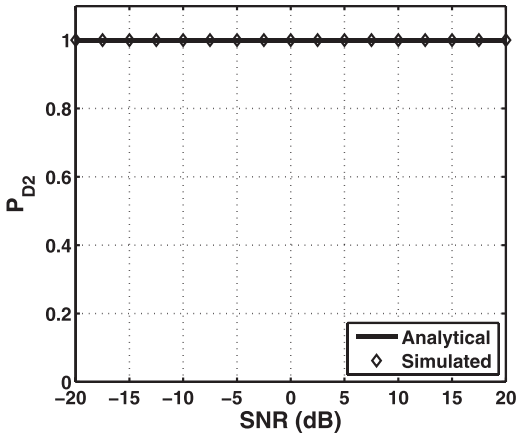

Fig. 5. Correct probability of d_2 in second layer of PCA, when $\hat{d}_1 = d_1$.

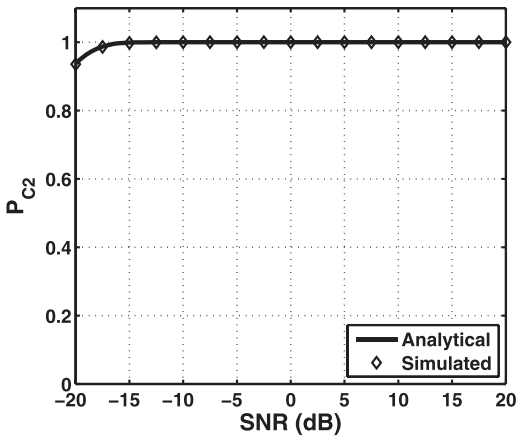

Fig. 6. Joint correct probability of d_2 and c_2 in second layer of PCA, when $\hat{d}_1 = d_1$.

For simplicity, we assume $\hat{d}_1 = d_1$ for the analysis of the second layer. According to the Appendix, the magnitude distribution of the sidelobe of $|G_n^{(2)}|$ with $n \neq d_2$ is given by

$$f(l_s) = \frac{l_s}{K_1 K_2/2} e^{-l_s^2/K_1 K_2}, \tag{53}$$

where $l_s \geq 0$.

On the other hand, the magnitude distribution of $|G_n^{(2)}|$ with $n = d_2$ is denoted by

$$f(l_p) = \frac{l_p}{\sigma_{p2}^2} e^{-(l_p^2+\mu_{\text{Re2}}^2)/2\sigma_{p2}^2} \cdot I_0\left(\frac{l_p \mu_{\text{Re2}}}{\sigma_{p2}^2}\right), \tag{54}$$

where $l_p \geq 0$.

Similarly, for a given l_p, the correct probability of d_2 is the probability that l_p is greater than all the other $K_2 - 1$ sidelobes, which is denoted by

$$\text{P}_\text{d}(l_p) = \left(1 - \exp\left(-\frac{l_p^2}{K_1 K_2}\right)\right)^{K_2-1}. \tag{55}$$

Considering the distribution of l_p, the correct probability of d_2, i.e., $\hat{d}_2 = d_2$, is given by

$$\text{P}_{\text{D2}} = \int_0^\infty \text{P}_\text{d}(l_p) f(l_p) dl_p. \tag{56}$$

Furthermore, the joint distribution of the magnitude and phase of $G_{d_2}^{(2)}$ is given by

$$f(l_p, \vartheta) = \frac{l_p}{2\pi\sigma_{p2}^2} \exp\left(-\frac{l_p^2 + \mu_{\text{Re2}}^2 - 2l_p\mu_{\text{Re2}}\cos\vartheta}{2\sigma_{p2}^2}\right), \tag{57}$$

where $-\pi \leq \vartheta \leq \pi$.

Hence, the joint probability of the correct d_2 and c_2 is denoted by

$$\text{P}_{\text{C2}} = 2 \cdot \int_0^{\frac{\pi}{M_2}} \int_0^\infty \text{P}_\text{d}(l_p) f(l_p, \vartheta) dl_p d\varphi. \tag{58}$$

The correct probabilities of P_{D2} and P_{C2} are shown in Figs. 5 and 6, respectively. We use the same parameters for the first layer and take $K_2 = 2^5 + 1$ and $M_2 = 2^5 - 1$ in the second layer. Still, the analytical results are consistent with the simulated values in both figures. The improvement brought by the second layer is significant, because the correct probability of d_2 approaches one for SNR from -20 to 20 dB in Fig. 5. Moreover, the joint correct probability of d_2 and c_2 is greater than 0.9 when SNR ≥ -20 dB in Fig. 6.

Similarly, the STD of $\hat{c}_2$ with the condition that $\hat{d}_2 = d_2$ is derived by

$$\sigma_\vartheta = \left[\frac{1}{\text{P}_{\text{D2}}} \int_{-\pi}^{\pi} \vartheta^2 \cdot \int_0^\infty \text{P}_\text{d}(l_p) f(l_p, \vartheta) dl_p d\vartheta\right]^{1/2}. \tag{59}$$

In Fig. 7, the STD is much less than one chip for SNR ≥ -20 dB and approaches zero when SNR ≥ 5 dB. The noise robustness of the multilayer PCA is thus verified, especially in the case of low SNR, as comparing Figs. 4 and 7.

To further explore the acquisition performance of PCA, we use the P code, which is a category of long PN sequences used in GNSS applications [15]. Let the code length be $N = 2^{16} - 1$. Three PCA

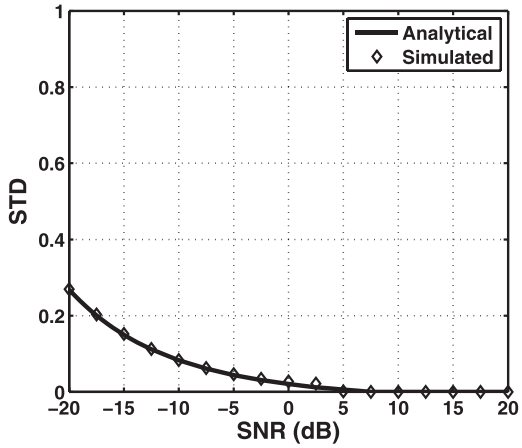

Fig. 7. STD of $\hat{c}_2$ in second layer of PCA, when $\hat{d}_1 = d_1$ and $\hat{d}_2 = d_2$.

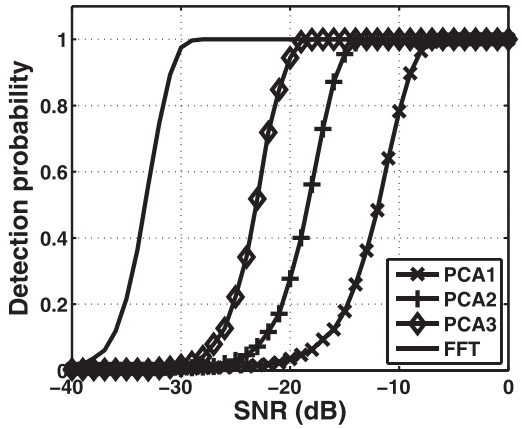

Fig. 8. Detection probability of P code of length $N = 2^{16} - 1$ with PCA schemes: two-layer PCA1 with $(K_1, M_1) = (2^8 + 1, 2^8 - 1)$ and $(K_2, M_2) = (2^4 + 1, 2^4 - 1)$, two-layer PCA2 with $(K_1, M_1) = ((2^8 + 1) \cdot (2^2 + 1), (2^4 + 1) \cdot (2^2 - 1))$ and $(K_2, M_2) = (2^4 + 1, 2^2 - 1)$, and single-layer PCA3 with $(K, M) = ((2^8 + 1) \cdot (2^4 + 1), (2^2 + 1) \cdot (2^2 - 1))$ and N-point FFT-based acquisition.

schemes are applied to the P code acquisition: the two-layer PCA1 with $(K_1, M_1) = (2^8 + 1, 2^8 - 1)$ and $(K_2, M_2) = (2^4 + 1, 2^4 - 1)$, the two-layer PCA2 with $(K_1, M_1) = ((2^8 + 1) \cdot (2^2 + 1), (2^4 + 1) \cdot (2^2 - 1))$ and $(K_2, M_2) = (2^4 + 1, 2^2 - 1)$, and the single-layer PCA3 with $(K, M) = ((2^8 + 1) \cdot (2^4 + 1), (2^2 + 1) \cdot (2^2 - 1))$. The performance is shown in Fig. 8. Note that only the dominant detection probability P_{D1} of PCA schemes is provided for simplicity. The performance of the N-point FFT-based acquisition is also shown in Fig. 8 for comparison. According to the detection probability in Fig. 8, FFT-based method outperforms PCA schemes in low SNR. The PCA, on the other hand, provides flexibility for applications in different ambient SNR. The reduction of computation of these PCA schemes over the FFT-based method will be discussed in the following section.

VI. COMPUTATIONS OF PCA

The computations of PCA are studied and compared with that of FFT-based acquisition. Here, we assume the computations regarding the local sequence are omitted, because it can be calculated in advance. For the first-layer process of PCA, the derivation of the phasors of the input sequence, as shown in (16), requires $K_1 \cdot (M_1 - 1)$ additions. Also, the calculation of $G_m^{(1)}$ in (25) requires $K_1 \cdot K_1$ additions (subtractions) for the phase difference and $K_1(K_1 - 1)$ additions for the sum of phasors. Regarding the computing of the complex phase in (22), the coordinate rotation digital computer (CORDIC), for computing using shifts and additions, can be used [16]. In CORDIC, let P_1 denote the parameter associated with the required phase resolution in the first layer, i.e., $\tan^{-1} \frac{1}{2^{P_1}} \leq \frac{2\pi}{M_1}$ for (28). For example, when $P_1 = 8$, the phase resolution is sufficient for $M_1 = 2^{10} - 1$. As a result, $3K_1P_1$ additions are needed for computing the complex phases in (22). Hence, the overall addition in the first layer is $K_1 \cdot (M_1 + 2K_1 - 2 + 3P_1)$. For the second-layer process, $K_1K_2 \cdot (M_2 - 1)$ additions are needed for the input phasor and $K_1 \cdot K_2^2 + K_1K_2(K_2 - 1)$ additions for computing (32) and (33). In addition, assume that the required phase resolution in the second layer is $\tan^{-1} \frac{1}{2^{P_2}} \leq \frac{2\pi}{M_2}$, we then need $3K_1K_2P_2$ additions for the complex phase using the CORDIC computing. Therefore, $K_1K_2 \cdot (M_2 + 2K_2 - 2 + 3P_2)$ additions are required in the second layer. Note that the parameters regarding phase resolution in CORDIC, i.e., P_1 and P_2 should be at least large enough to distinguish between the adjacent phases in the multilayer PCA. Otherwise, the accuracy of phase estimation and subsequent estimation of c will be bounded by the resolution of CORDIC, which would result in a bias in the ultimate code phase acquisition.

TABLE I
Computations of Three PCA Schemes with Performance Illustrated in Fig. 8 for P Code of Length $N = 2^{16} - 1$

Method	Operation Multiplications	Additions
PCA1	0	$7N$
PCA2	0	$68N$
PCA3	0	$585N$
FFT-based method	$32N$	$32N$

To be more specific, we consider the computations involved in acquisition schemes PCA1, PCA2, and PCA3, which have performance illustrated in Fig. 8, for P code of length $N = 2^{16} - 1$. Here, we use $P_1 = 8$ and $P_2 = 4$. According to the summary of computation complexity in Table I, no multiplication is used in the PCA schemes, but the number of additions increases with the number of partitions K. Computations of the FFT-based method are also provided in Table I for comparison. The FFT-based method substantially requires $2N \log_2 N$ multiplications and additions because of $N \log_2 N$ multiplications and additions on both the FFT for the input sequence and the IFFT for the conversion of a real sequence from complex phasors [3–5]. Note that PCA1 uses even fewer additions than the FFT-based acquisition. In particular, when the two-layer PCA scheme with $K_1 = 2^{n/2} + 1$, $M_1 = 2^{n/2} - 1$,

TABLE II
Computations of the Two-Layer PCA with $K_1 = 2^{n/2} + 1,\ M_1 = 2^{n/2} - 1,\ K_2 = 2^{n/4} + 1$, and $M_2 = 2^{n/4} - 1$ and the FFT-Based Method for the PN Sequence of an Extremely Large Length $N = 2^n - 1$

Method	Operation Multiplications	Additions
PCA	0	$6N$
FFT-based method	$2N \log_2 N$	$2N \log_2 N$

K_2=$2^{n/4}$+1, and $M_2 = 2^{n/4} - 1$ for a PN sequence of an extremely large $N = 2^n - 1$ is implemented, the computations for the phase become relatively insignificant, and then approximately $3N$ additions are required for both the first and the second layer in PCA. The computational burden is significantly reduced to $6N$ additions in the two-layer PCA as compared with $2N \log_2 N$ multiplications and additions in the FFT-based method, as indicated in Table II. Because of its superior computational efficiency, PCA may be applied to the unique pattern search in a long sequence. Potential applications include the long PN code acquisition, such as P(Y) code and spot beam M code, and revealing an encrypted PN code in GNSS and the satellite communication field [8, 17–20].

VII. CONCLUSIONS

In this paper, the PCA method using the phase difference of complex phasors for the PN sequence acquisition is proposed. The PCA requires only complex additions but no complex multiplications. In addition, the acquisition performance can be improved via the use of the multilayer scheme that also provides the inherent error detection capability. Segmentation, phasor acquisition, and the multilayer scheme for the PCA algorithm are introduced in Section IV, and the analysis is conducted in Section V. In the demonstrated case using MLS of length $N = 2^{20} - 1$ in the two-layer scheme of PCA, the correct segment of the first layer is obtained with probability approaching one when SNR > -15 dB, as shown in Fig. 2. As we identify the correct segment of the first layer, the acquisition performance attains the correct probability greater than 0.9 for SNR ≥ -20 dB after the second layer, as shown in Fig. 6. It is noteworthy that PCA requires much less computation than the FFT-based approach as discussed in Section VI and demonstrated in Tables I and II. Hence, for applications having high SNR margins, such as the spot beam signaling [18], the secure telemetry, tracking and command link [19], or the processing of denoised signals, the use of PCA will significantly reduce the computation, namely, the complex multiplications are eliminated, as compared with the FFT-based method. Moreover, according to Table I, the PCA method also has flexibility in selecting the number of layers and partitions to reduce the computation based on SNR margins, as shown in Fig. 8, whereas the FFT-based acquisition requires a fixed number of computations regardless of SNR. The superior performance on the computation grants the PCA an effective method when the length of a sequence is so large that the FFT-based acquisition is infeasible. Finally, it is worth mentioning that the SNR performance of PCA regarding the detection probability can be improved when a one-bit quantized input sequence in (16) is replaced by a multibit quantized version. The improvement is obtained by the reduction of quantization loss. However, the price is the computational complexity because the multiplications are required in (16). Further investigations may be interesting but beyond the scope of this work.

APPENDIX. MAGNITUDE AND PHASE DISTRIBUTION OF G_m

The distribution of G_m in the first layer, $G_m^{(1)}$, is derived first. We rewrite (38) as

$$w_n = x_n + \beta_n \bar{x}_n \tag{60}$$

where $\beta_n \in \{0, 2\}$ and $\bar{x}_n$ denotes the inverse of x_n.

In (60), when $\beta_n = 2$, we have $w_n = \bar{x}_n$, indicating that an error occurs because of noise ζ_n. The corresponding error probability is given by

$$\begin{aligned} P_e &= \Pr(\beta_n = 2) \\ &= Q(1/\sigma_n), \end{aligned} \tag{61}$$

where $Q(z) = \int_z^\infty e^{-x^2/2} dx$.

We can represent (41) as

$$\begin{aligned} W_i &= \sum_{n=0}^{M_1-1} w_{nK_1+i} \alpha^{-n} \\ &= X_i + \sum_{n=0}^{M_1-1} \beta_{nK_1+i} \bar{x}_{nK_1+i} \alpha^{-n}, \end{aligned} \tag{62}$$

where $X_i = \sum_{n=0}^{M_1-1} x_{nK_1+i} \alpha^{-n}$ is assumed to be fixed.

Let $E\{z\}$ denote the expected value of z. The mean value of W_i is obtained by

$$\begin{aligned} E\{W_i\} &= E\left\{ X_i + \sum_{n=0}^{M_1-1} \beta_{nK_1+i} \bar{x}_{nK_1+i} \alpha^{-n} \right\} \\ &= X_i + \sum_{n=0}^{M_1-1} E\{\beta_{nK_1+i}\} \bar{x}_{nK_1+i} \alpha^{-n} \\ &= X_i + 2P_e \cdot \sum_{n=0}^{M_1-1} \bar{x}_{nK_1+i} \alpha^{-n} \\ &= (1 - 2P_e) \cdot X_i, \end{aligned} \tag{63}$$

where $E\{\beta_{nK_1+i}\} = 2P_e$ and $\sum_{n=0}^{M_1-1} \bar{x}_{nK_1+i} \alpha^{-n} = -X_i$.

Furthermore, to obtain the variance of W_i, we calculate

$$\begin{aligned}
E\{W_i W_i^*\} &= E\left\{ \left(X_i + \sum_{n=0}^{M_1-1} \beta_{nK_1+i} \bar{x}_{nK_1+i} \alpha^{-n} \right) \right. \\
&\quad \left. \cdot \left(X_i + \sum_{m=0}^{M_1-1} \beta_{mK_1+i} \bar{x}_{mK_1+i} \alpha^{-m} \right)^* \right\} \\
&= X_i X_i^* + X_i \cdot \sum_{m=0}^{M_1-1} E\{\beta_{mK_1+i}\} \bar{x}_{mK_1+i} \alpha^m + X_i^* \\
&\quad \cdot \sum_{n=0}^{M_1-1} E\{\beta_{nK_1+i}\} \bar{x}_{nK_1+i} \alpha^{-n} \\
&\quad + E\left\{ \left(\sum_{n=0}^{M_1-1} \beta_{nK_1+i} \bar{x}_{nK_1+i} \alpha^{-n} \right) \right. \\
&\quad \left. \cdot \left(\sum_{m=0}^{M_1-1} \beta_{mK_1+i} \bar{x}_{mK_1+i} \alpha^{m} \right) \right\} \\
&= |X_i|^2 - 2P_e \cdot X_i X_i^* - 2P_e \cdot X_i^* X_i \\
&\quad + \sum_{\substack{n=0 \\ m=n}}^{M_1-1} E\{\beta_{nK_1+i} \beta_{mK_1+i}\} \bar{x}_{nK_1+i} \bar{x}_{mK_1+i} \alpha^{m-n} \\
&\quad + E\left\{ \sum_{n=0}^{M_1-1} \beta_{nK_1+i} \bar{x}_{nK_1+i} \alpha^{-n} \sum_{\substack{m=0 \\ m\neq n}}^{M_1-1} \beta_{mK_1+i} \bar{x}_{mK_1+i} \alpha^{m} \right\} \\
&\approx |X_i|^2 - 4P_e |X_i|^2 + 4P_e \sum_{\substack{n=0 \\ m=n}}^{M_1-1} \bar{x}_{nK_1+i} \bar{x}_{mK_1+i} \alpha^{m-n} \\
&= |X_i|^2 - 4P_e |X_i|^2 + 4P_e M_1, \qquad (64)
\end{aligned}$$

where $E\left\{ \sum_{n=0}^{M_1-1} \beta_{nK_1+i} \bar{x}_{nK_1+i} \alpha^{-n} \sum_{\substack{m=0 \\ m\neq n}}^{M_1-1} \beta_{mK_1+i} \bar{x}_{mK_1+i} \alpha^{m} \right\} \approx 0$ and $E\{\beta_{nK_1+i} \beta_{mK_1+i}\} = 4P_e$, when $m = n$.

By using (63) and (64), the variance of W_i is derived by

$$\begin{aligned}
Var\{W_i\} &= E\{|W_i|^2\} - (|E\{W_i\}|)^2 \\
&= E\{W_i W_i^*\} - E\{W_i\} \cdot (E\{W_i\})^*. \\
&= |X_i|^2 - 4P_e |X_i|^2 + 4P_e M_1 - ((1-2P_e)X_i) \\
&\quad \cdot ((1-2P_e)X_i)^* \\
&= 4P_e M_1 - 4P_e^2 |X_i|^2. \qquad (65)
\end{aligned}$$

It is reasonable to assume that $\{x_{nK_1+i}\}$ involved in X_i is a PN sequence of length M_1. Similar to (8), we have

$$|X_i|^2 \approx M_1 + 1. \qquad (66)$$

Let the code phase shift between input and local MLS be $q = c_1 K_1 + d_1$. Considering the sidelobe of $|G_m^{(1)}|$, i.e., $m \neq d_1$, in (43), the phases $\psi_{i,m}$ can be considered to be uniformly distributed between $-\pi$ and π. According to [21], the magnitude distribution of $|G_m^{(1)}|$, denoted by r_s, can be modeled using Rayleigh distribution, given as

$$f(r_s) = \frac{r_s}{K_1/2} e^{-r_s^2/K_1}, \qquad (67)$$

where $r_s \geq 0$.

On the other hand, for the $|G_m^{(1)}|$ with $m = d_1$, (43) is represented by

$$\begin{aligned}
G_{d_1}^{(1)} &= \sum_{i=0}^{K_1-1} e^{j\psi_{i,m}} \\
&= \sum_{i=0}^{K_1-1} e^{j\frac{2\pi}{M_1} c_1 + \Delta\phi_i}, \qquad (68)
\end{aligned}$$

where $\Delta\phi_i$ denotes the phase error induced by noise.

Without loss of generality, we assume $c_1 = 0$. Then, (68) becomes

$$G_{d_1}^{(1)} = \sum_{i=0}^{K_1-1} e^{j\Delta\phi_i}. \qquad (69)$$

The $\Delta\phi_i$ denotes the phase difference between the input phasor W_i and local phasor Y_i caused by noise. Because we have the mean and variance of W_i in (63) and (65), according to [21, Sec. 4.4], the distribution of $\Delta\phi_i$ can be approximated by

$$f(\Delta\phi_i) = \frac{1}{2\pi} \mathrm{e}^{-\rho} \left[1 + G\sqrt{\pi} \exp(G^2)(1 + \mathrm{erf}(G)) \right], \qquad (70)$$

where $\rho = \frac{(E\{W_i\})^2}{Var\{W_i\}}$, $G = \sqrt{\rho}\cos(\Delta\phi_i)$, and $-\pi \leq \Delta\phi_i \leq \pi$.

Moreover, to obtain the magnitude distribution of $G_{d_1}^{(1)}$, (69) is reformulated by

$$\begin{aligned}
G_{d_1}^{(1)} &= \sum_{i=0}^{K_1-1} e^{j\Delta\phi_i} \\
&= \sum_{i=0}^{K_1-1} \cos(\Delta\phi_i) + j \sum_{i=0}^{K_1-1} \sin(\Delta\phi_i) \\
&= \Gamma_{\mathrm{Re}} + j\Gamma_{\mathrm{Im}}, \qquad (71)
\end{aligned}$$

where $\Gamma_{\mathrm{Re}} = \sum_{i=0}^{K_1-1} \cos(\Delta\phi_i)$ and $\Gamma_{\mathrm{Im}} = \sum_{i=0}^{K_1-1} \sin(\Delta\phi_i)$.

We assume that each $\cos(\Delta\phi_i)$ and $\sin(\Delta\phi_i)$ are independent and identically distributed random variables. Let $\mathcal{N}(\mu, \sigma^2)$ denote the normal distribution function with mean μ and variance σ^2. By the central limit theorem, Γ_{Re} and Γ_{Im} can be approximated by two normal distributions $\mathcal{N}\left(\mu_{\mathrm{Re1}}, \sigma_{\mathrm{Re1}}^2\right)$ and $\mathcal{N}\left(\mu_{\mathrm{Im1}}, \sigma_{\mathrm{Im1}}^2\right)$, respectively, and the parameters are obtained by

$$\begin{aligned}
\mu_{\mathrm{Re1}} &= E\left\{ \sum_{i=0}^{K_1-1} \cos(\Delta\phi_i) \right\} \\
&= \sum_{i=0}^{K_1-1} E\{\cos(\Delta\phi_i\} \qquad (72)
\end{aligned}$$

$$\begin{aligned}
\sigma_{\mathrm{Re1}}^2 &= Var\left\{ \sum_{i=0}^{K_1-1} \cos(\Delta\phi_i) \right\} \\
&= \sum_{i=0}^{K_1-1} Var\{\cos(\Delta\phi_i)\} \qquad (73)
\end{aligned}$$

$$\mu_{\text{Im1}} = \sum_{i=0}^{K_1-1} E\{\sin(\Delta\phi_i)\} \tag{74}$$

$$\sigma^2_{\text{Im1}} = \sum_{i=0}^{K_1-1} Var\{\sin(\Delta\phi_i)\}. \tag{75}$$

Numerically, we find $\mu_{\text{Re1}} \neq 0$, $\mu_{\text{Im1}} = 0$, and $\sigma^2_{\text{Re1}} \cong \sigma^2_{\text{Im1}}$. For simplicity, let $\sigma^2_{p1} = (\sigma^2_{\text{Re1}} + \sigma^2_{\text{Im1}})/2$. According to [21], the magnitude of $G^{(1)}_{d_1}$, denoted by r_p, can be modeled by Rice distribution given as

$$f(r_p) = \frac{r_p}{\sigma^2_{p1}} e^{-(r_p^2+\mu^2_{\text{Re1}})/2\sigma^2_{p1}} \cdot I_0\left(\frac{r_p\mu_{\text{Re1}}}{\sigma^2_{p1}}\right), \tag{76}$$

where $r_p \geq 0$ and $I_0(\cdot)$ is the modified Bessel function of the first kind with order zero.

In addition, the joint magnitude of phase distribution of $G^{(1)}_{d_1}$ is given by

$$f(r_p, \varphi) = \frac{r_p}{2\pi\sigma^2_{p1}} \exp\left(-\frac{r_p^2 + \mu^2_{\text{Re1}} - 2r_p\mu_{\text{Re1}}\cos\varphi}{2\sigma^2_{p1}}\right), \tag{77}$$

where $-\pi \leq \varphi < \pi$.

The derivation of magnitude and phase distribution of G_m can be applied to other layers. For example, for the sidelobe of $|G^{(2)}_n|$ with $n \neq d_2$, the phases $\psi_{i,t+n}$ in (52) can be considered to be uniformly distributed between $-\pi$ and π. The distribution of sidelobe of $|G^{(2)}_n|$, denoted by l_s, can then be modeled by

$$f(l_s) = \frac{l_s}{K_1K_2/2} e^{-l_s^2/K_1K_2}, \tag{78}$$

where $l_s \geq 0$.

Moreover, let

$$\mu_{\text{Re2}} = \sum_{i=0}^{K_1-1}\sum_{t=0}^{K_2-1} E\{\cos(\psi_{i,t+d_2})\} \tag{79}$$

$$\sigma^2_{\text{Re2}} = \sum_{i=0}^{K_1-1}\sum_{t=0}^{K_2-1} Var\{\cos(\psi_{i,t+d_2})\} \tag{80}$$

$$\mu_{\text{Im2}} = \sum_{i=0}^{K_1-1}\sum_{t=0}^{K_2-1} E\{\sin(\psi_{i,t+d_2})\} \tag{81}$$

$$\sigma^2_{\text{Im2}} = \sum_{i=0}^{K_1-1}\sum_{t=0}^{K_2-1} Var\{\sin(\psi_{i,t+d_2})\}. \tag{82}$$

The magnitude of $G^{(2)}_n$ with $n = d_2$, denoted by l_p, is modeled by

$$f(l_p) = \frac{l_p}{\sigma^2_{p2}} e^{-(l_p^2+\mu^2_{\text{Re2}})/2\sigma^2_{p2}} \cdot I_0\left(\frac{l_p\mu_{\text{Re2}}}{\sigma^2_{p2}}\right), \tag{83}$$

where $l_p \geq 0$ and $\sigma^2_{p2} = (\sigma^2_{\text{Re2}} + \sigma^2_{\text{Im2}})/2$.

In addition, the joint magnitude of phase distribution of $G^{(2)}_{d_2}$ is denoted by

$$f(l_p, \vartheta) = \frac{l_p}{2\pi\sigma^2_{p2}} \exp\left(-\frac{l_p^2 + \mu^2_{\text{Re2}} - 2l_p\mu_{\text{Re2}}\cos\vartheta}{2\sigma^2_{p2}}\right), \tag{84}$$

where $-\pi \leq \vartheta < \pi$.

REFERENCES

[1] Polydoros, A., and Weber, C. L.
A unified approach to serial search spread-spectrum code acquisition—part I: general theory.
IEEE Transactios on Communications, **32**, 5 (May 1984), 542–549.

[2] Polydoros, A., and Weber, C. L.
A unified approach to serial search spread-spectrum code acquisition—part II: a matched-filter receiver.
IEEE Transactions on Communications, **32**, 5 (May 1984), 550–560.

[3] Cooley, J. W., and Tukey, J. W.
An algorithm for the machine calculation of complex Fourier series.
Mathematics of Computation, **19** (Apr. 1965), 297–301.

[4] Cochran, W. T., Cooley, J. W., Favin, D. L., Helms, H. D., Kaenel, R. A., Lang, W. W., Maling, G. C., Jr., Nelson, D. E., Rader, C. M., Welch, P. D.
What is the fast Fourier transform?
Proceedings of the IEEE, **55**, 10 (Jun. 1967), 1664–1674.

[5] Oppenheim, A. V., and Schafer, R. W.
Discrete-Time Signal Processing, Englewood Cliffs, NJ: Prentice Hall, 1989.

[6] Cheng, U., Hurd, W. J., and Statman, J. I.
Spread-spectrum code acquisition in the presence of Doppler shift and data modulation.
IEEE Transactions on Communications, **38**, 2 (Feb. 1990), 241–250.

[7] van Nee, D. J. R., and Coenen, A. J. R. M.
New Fast GPS code-acquisition technique using FFT.
Electronics Letters, **27**, 2 (Jan. 1991), 158–160.

[8] Lin, D. M., Tsui, J. B.-Y., and Howell, D.
Direct P(Y)-code acquisition algorithm for software GPS receivers. Presented at the ION GPS 1999, Nashville, TN, Sep. 1999.

[9] Sagiraju, P. K., Agaian, S., and Akopian, D.
Reduced complexity acquisition of GPS signals for software embedded application.
IEE Proceedings Radar, Sonar and Navigation, **153**, 1 (Feb. 2006), 69–78.

[10] Akopian, D.
Fast FFT based GPS satellite acquisition methods.
IEE Proceedings Radar Sonar and Navigation, **152**, 4 (Aug. 2005), 277–286.

[11] Lin D. M., and Tsui, J. B.-Y.
Comparison of acquisition methods for software GPS receiver. Presented at the ION GPS 2000, Salt Lake City, UT, Sep. 2000.

[12] Pany, T., Gohler, E., Irsigler, M., and Winkel, J.
On the state-of-the-art of real-time GNSS signal acquisition—a comparison of time and frequency domain methods.
Presented at the International Conference Indoor Positioning and Indoor Navigation, Zurich, Switzerland, Sep. 2010.

[13] Moghaddam, A. R. A., Watson, R., Lachapelle, G., and Nielsen, J.
Exploiting the orthogonality of L2C code delays for a fast acquisition. Presented at the ION GNSS 2006, Fort Worth, TX, Sep. 2006.

[14] Juang, J.-C., and Chen, Y.-H.
Global navigation satellite system signal acquisition using multi-bit code and a multi-layer search strategy.
IET Radar, Sonar & Navigation, **4**, 5 (Oct. 2010), 673–684.

[15] Kaplan, E. D., and Hegarty, C. J.
Understanding GPS: Principles and Applications, Norwood, MA: Artech House, 2006.

[16] Volder, J. E.
The CORDIC trigonometric computing technique.
IRE Transactions on Electronic Computers, **EC-8**, 3 (Sep. 1959), 330–334.

[17] Yang, C., Vasquez, M. J. and Chaffee, J.
Fast direct P(Y)-code acquisition using XFAST. Presented at the ION GPS 1999, Nashville, TN, Sep. 1999.

[18] Barker, B. C., Betz, J. W., Clark, J. E., Correia, J. T., Gillis, J. T., Lazar, S., Rehborn, K. A., and Straton, J. R.
Overview of the GPS M Code Signal.
In *Procedings of the 2000 National Technical Meeting of the Institute of Navigation*, Anaheim, CA, Jan. 2000.

[19] Simone, L., Fittipaldi, G., and Sanchez, I. A.
Fast acquisition techniques for very long PN codes for on-board secure TTC transponders.
In *Proceedings of the IEEE Military Communications Conference*, Baltimore, MD, Nov. 2011, 1748–1753.

[20] Gao, G. X. Chen, A., Lo, S., Lorenzo, D., Walter, T., and Enge, P.
Compass-M1 broadcast codes in E2, E5b, and E6 frequency bands.
IEEE Journal of Selected Topics in Signal Processing, **3**, 4 (Aug. 2009), 599–612.

[21] Beckmann, P.
Probability in Communication Engineering. New York: Harbrace, 1967.

Wan-Hsin Hsieh is currently a senior research engineer of Applied Research Department in St. Jude Medical, Inc., based in Taipei, Taiwan. He received his Ph.D. degree in electrical engineering from National Chiao Tung University, Hsinchu, Taiwan. From 2012 to 2013, he was with the Division of Sleep and Circadian Disorders at Brigham and Women's Hospital, Harvard Medical School, where he was a postdoctoral research fellow in the Medical Biodynamics Program. His research interests include digital signal processing, biomedical signal processing, and nonlinear dynamics in medicine.

Chieh-Fu Chang received his Ph.D. degree in electrical and computer engineering from Purdue University, West Lafayette, IN. He is currently an associate researcher at the Electrical Engineering Division of the National Applied Research Laboratory - National Space Organization in Taiwan. His current research interests include digital receivers, signal processing, satellite communications, and remote sensing instrument.

[no photo available]

Ming-Seng Kao (S'89—M'90) was born in Taipei, Taiwan, Republic of China, in 1959. He received a B.S.E.E. degree from the National Taiwan University in 1982, his M.S. degree in optoelectronics from the National Chiao Tung University in 1986, and a Ph.D. degree in electrical engineering from the National Taiwan University in 1990. From 1986 to 1987, he was an assistant researcher at the Telecommunications Laboratories, Chung-Li, Taiwan. In 1990, he joined the faculty of National Chiao Tung University, Hsinchu, Taiwan, where he is now a professor in the Communication Engineering Department. Between 1993 and 1994, he was a visiting professor at the Swiss Federal Institute of Technology, Zurich, Switzerland, where he worked in optical communications. In 2003, he was a visiting professor at the Nanyang Technological University, Singapore, where he investigated optical devices and networking. He is currently interested in wireless communications and digital receivers.